# Mechanical behavior and fracture surface characterization of liquid-phase sintered Cu-Sn powder alloys

**Ahmed E. Nassef[1], A.I. Alateyah[2], Medhat A. El-Hadek[1], W. H. El-Garaihy[2,3*]**

[1]*Department of Production & Mechanical Design, Faculty of Engineering, Port-Said University, 23 July St., Port-Said, 42523, Egypt*
[2]*Mechanical Engineering Department, Unizah College of Engineering, Qassim University, King Abdulaziz St., 51911, Kingdom of Saudi Arabia*
[3]*Mechanical Engineering Department, Faculty of Engineering, Suez Canal University, El Salam district, Ismailia 41522, Egypt*

[*]Corresponding author, Tel: (+966) 551108490; E-mail: W.Nasr@qu.edu.sa

## Abstract

In this study, elemental Cu and Sn powder were mechanically mixed forming different Cu-Sn alloys. To ensure uniformity of the particle shapes, the *Cu*, and *Sn* were mechanically milled and mixed in an agate rock mortar, with high energy ball mill for half an hour, with different weight ratios according to the composition design. The milling of the powders resulted in uniform sphere-like particles for *Cu–Sn* alloys. Hot compaction was performed in a single acting piston cylinder arrangement at room temperature. All hot pressed MMCs were heat-treated at about 550°C to allow the atoms to diffuse randomly into a uniform solid solution, as liquid phase sintering. Vickers micro-hardness measurements were carried out for the hot-pressed *Cu–Sn* alloys. Cylindrical specimens of aspect ratio of $h_o/d_o = 1.5$ were tested under frictionless conditions at the compression platen interface. Charpy transverse rupture strength had been used to determine the fracture strength of the different Cu-Sn alloys. Fracture surface features of the different Cu-Sn alloys were characterized using scanning electron microscopy. It had been found that, the *85%Cu–15% Sn* alloy revealed an increase of hardness values, a decrease of the yield strength, and an increase in the impact energy by 26.2, 23, and 18.7%; respectively, compared with the Sn-free alloy. The Cu-Sn alloys showed an apparently classical inclined fracture surface, at about 45° with the applied stress axis, which was similar to what's obtained for a diversity of hard metals. Copyright © 2017 VBRI Press.

**Keywords:** Cu-Sn alloy, metal matrix composite, strengthening, fracture mechanics.

## Introduction

Cu and Cu alloys are crucial materials, which are extensively used in industry as conductive materials in numerous electrical and electronic applications. The tendency for their extensive industrial use refers to their superior electrical conductivity, minimum cost, exceptional mechanical properties, simplicity of material processing, and outstanding corrosion and wear resistance [1-2].

Cu-Sn alloy powders is a type of Cu alloys, which are adopted broadly in a vast variety of uses due to their excellent thermal and electrical conductivity, high strength, outstanding wear resistances and corrosion protection, decent malleability, and good ductility and solderability. Some of their most common utilizations are electronic industries and solders, lithium ion batteries, shape memory applications, wear and corrosion protection, decorative finishing of various metallic articles and medical apparatus, self-lubricant machines,

and metal coatings; moreover, Cu-Sn alloy thin films are commonly used, as a precursor layer, in thin film semiconductor absorber fabrication [3-12]. In addition, Cu–Sn alloy systems has revealed outstanding properties and desirability of their use in $Cu_6Sn_5$ and $Cu_3Sn$; as a result of their distinctive intermetallic compounds (IMCs) characteristics, where the tendency increased towards power density, multi-functionalization and miniaturization, and materials with high-melting-points to reach high temperature capabilities and stability for microelectronic and circuit interconnection devices [13-16].

Cu-Sn alloys are obtained by powder processing with the assistance of liquid phase, which is used for the formation of various materials [17]. Liquid-phase sintering (LPS) is a crucial densification process used to achieve multiple-phase components and materials with high-performance [18-19]. LPS has many processing advantages over other sintering processes; such as solid-

state sintering. This competitive edge includes: less required sintering temperatures and fast densification, cheaper elemental powders are needed against alloyed powders, and minimized microstructural coarsening; in addition, the diffusion, the bonding process, particle rearrangement, and pore elimination taking place in powder consolidation are ameliorated in LPS due to the utilization of a liquid phase resulted from adding an additive phase (A), which forms a low melting eutectic point with the base metal (B) [20- 27]. During heating in situ alloying between the powders creates a low melting point liquid, which assists in the powder densification process. Melting of the lower melting point component in the alloy (so called the binder) forms the liquid phase, and, subsequently, this liquid phase bonds the component with higher melting point. Continued heating and alloying alters the composition of the liquid until it isothermally solidifies [17]. This liquid which yielded from LPS spreads throughout the powder compact under capillary forces, causing particle rearrangement, enhanced mass transport and densification [20]. Capillary force provided by the liquid pulls solid grains together by spreading into the pores of the solid-liquid-pore structure and wetting the particles; at the same time, delivers a rapid diffusion rate whereas its motion eliminates pore; meanwhile, a softening takes place in the solid due to elevated temperature which aids further in densification [21, 25, 28-29]. As a result of grains sliding and rearrangement, a uniform shrinkage, densification, and contact flattening between touching grains occurs [29]. On the other hand, the difference in solid-pores density gives a buoyancy force; which could result in distortions on the pores; therefore, it is desirable to use smaller particles which would lead to an improved grain reshaping and repacking to a dense structure; due to the better dissolvability in the melt and consequently precipitation onto the larger grains [25]. Adopting LPS is not only driven surface energy minimization through the use of capillary forces but also the decrease of chemical potential via dissolving the original phases and the development of equilibrium solid phases [26]. Getting the best out the of this technique needs a significantly large capillary force from the wetting liquid, which would lead to a small initial particle size, mostly ranging from 1 µm to less [30].

Explanation of liquid phase sintering way of action could be summarized in three overlapping actions; as shown in **Fig. 1** for the case of two mixed powders, where a rearrangement and rapid shrinkage occurs for the solid material; meanwhile, a dissolution and re-precipitation takes place along with densification; moreover, an occurrence of coalescence when the liquid phase disappears [22-26].

In this paper, a novel study was carried out to explore the effects the liquid-phase sintering process on a hot-pressed Cu-based MMCs. Elemental Cu and Sn powder were mechanically mixed forming different Cu-Sn alloys. To ensure uniformity the *Cu* and *Sn* powders were mechanically milled using high energy ball mill. The effect of the Sn addition on the mechanical response was investigated on the hardness, compression response, transverse rupture strength, and fracture properties.
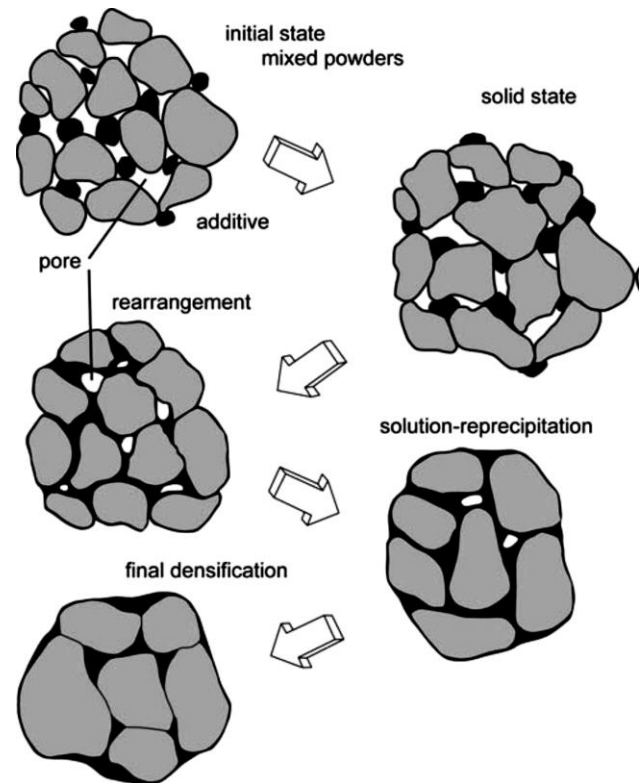


**Fig. 1.** A schematic of the microstructure changes during LPS [26].

## Experimental

### Materials

Elemental *Cu* and *Sn* have many wanted characteristics due to their strong ionic interatomic bonding. Powders with purity greater than 99%; with an average particle size less than 10 µm in diameter and manufactured by Alfa Aesar, USA, were used as the starting source materials.

### Material synthesis

The various powder components were mechanically mixed, to ensure uniformity of the particle shapes, forming nominal compositions of weight percentages as: 100%Cu–0%Sn, 95%Cu–5%Sn, 90%Cu–10%Sn, and 85%Cu–15% Sn. Mixing and milling of *Cu*, and *Sn* was accomplished through an agate rock mortar, with high energy ball milled for half an hour; with different weight ratios according to the composition design. The milling of powders resulted in uniform sphere-like particles, for *Cu–Sn* alloys.

The process starts with preparing the plating baths that contains the Sn particles of known weight using the electroless mixture solution and reducing agent. A uniform Cu film was formed on the Sn surface particles in about 10–15 min, which was deposited from the hypophosphite based solutions from the alkaline baths. In addition, a complexing agent; such as, citrate and ammonium salts were also used to increase the particulate bonding. The complexing agents has the function of preventing the precipitation of basic salts, in addition, it also affects the deposition rate and properties. The bath of

*ph* level was usually maintained in the range between 8 and 10, using ammonium hydroxide. Lower deposition rates resulted when the *ph* level was adjusted with sodium hydroxide; therefore, ammonium hydroxide was used for adjusting the *ph* of baths. The first bath was used to produce semi–bright Sn particles deposits containing 4% phosphorus; approximately. Deposition rates were increased with increased *ph* bath or hypophosphite concentration. The deposition rate in the first bath was increased from 5.6 μm/h to 10 μm/h at 85°C by simply adding organosulfur compound of 0.2 gm/cm$^3$ thiourea. The second bath contained less citrate than the first one, which resulted in a substantially greater deposition rate; however, the resulting deposits had inferior physical properties. The last bath was a typical acid electroless Sn particles plating bath, using a reducing agent, which was incapable of yielding Sn particles deposits from acidic solution. Electroless method is characterized by providing substantial cost minimization, ameliorating quality of the deposited materials, and minimizing cross–contamination. The weight of Cu coatings was estimated by the difference in weight between the graphite particles before and after the electroless coating process. Hot compaction was performed in a single acting piston cylinder arrangement at room temperature in order to get 30 mm diameter and 50 mm height of the green compact (aspect ratio h/d = 1.66), as shown in **Fig. 2**. The die bore was smeared with the intension of powders reducing die–wall friction; the desired weights of mixed composites were used for each compact. A hydraulic testing machine of 200 tons capacity was used to perform the compaction of the alloy powder with constant cross head speed of 2 mm/min.
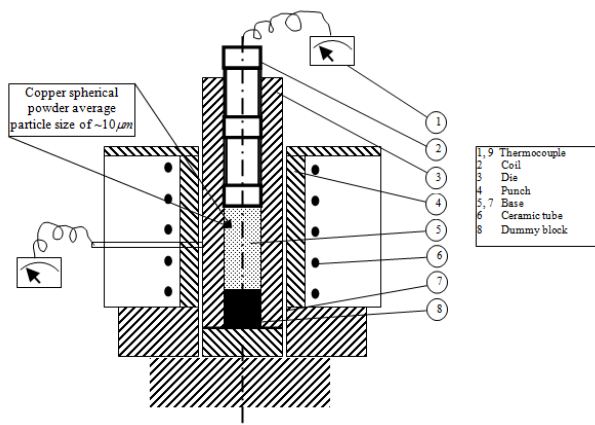


**Fig. 2.** Die setup of the hot compaction powder metallurgy pressing technique.

The height of the green compact was measured directly before and after ejecting from the die; the final height was also calculated from the load-displacement curve [31] and plotting of the dependence of relative density on the compaction pressure and analyze the obtained empirical curve within the framework of existing theories of powder pressing [32]. The die temperature was measured using a thermocouple, which was inserted through the die and kept near its cavity. The temperature was maintained at the required level with a tolerance of ±5°C. Different

mold temperatures were tested up to 550°C, at constant pressure of 314.38 MPa and constant crosshead speed of 2 mm/min. All hot pressed MMCs were heat-treated at about 550°C to allow the atoms to diffuse randomly into a uniform solid solution, as liquid phase sintering. The Sn melts to form a thin film surrounding the copper particles; therefore, enhances the alloying element bonding.

*Characterizations*

Hardness measurements were conducted on the polished surfaces of Cu-Sn alloys using digital metallic Vicker's hardness tester. Vickers micro-hardness measurements were carried out for the hot-pressed Cu–Sn alloys, using a load of 1 Kg for 15 sec dwell time, and indenter speed of 100μm/sec. Sample preparation for conducting the hardness test had been performed through consecutive steps of grinding using Buehler SiC grinding paper with grits of 240, 320, 400, 600, 800, and 1200 in existence of coolant (water). Two flat and parallel surfaces were polished using an aqueous 1% solution of ferric nitrate as a polishing media. To insure consistency and homogeneity throughout the material surface, a minimum of five readings were taken for each case and average values were recorded each time.

In addition, cylindrical specimens of aspect ratio of $h_o/d_o = 1.5$ ($h_o$ and $d_o$ were the original height and diameter of the specimen; respectively) were tested under frictionless conditions at the compression platen interface. The tests were carried out at room temperature using MTS Testing Machine (Model 610), fitted with a 160 KN load cell operating in the displacement control mode. The stress–strain responses of Cu–based alloys were measured from a uniaxial compression test, performed according to ASTM standard of E-9 for metals. The cross-head speed was adjusted to give an average strain rate of $7.6 \times 10^{-4}$ s$^{-1}$ across the specimen height. The test was terminated when the first surface crack was observed. Tests were repeated with three samples for each experiment.

Charpy transverse rupture strength (TRS) is one of the most common methods for determining the fracture strength as it is met during a three-point bending test. All Cu-Sn alloys samples were compacted into rectangular specimen's dimensions of 30x12x6.0 mm, at a compaction pressure of 30 Mpa. The rupture test was performed using compression testing machine and a test fixture, according to MPIF. The specimens were placed between the platens of the three-point bending testing machine and the load was applied at constant rate of 2.5 mm/min, until the specimens was fractured. To ensure consistently, the tests were repeated with three samples for each experiment. Fracture surface features of the different Cu-Sn alloys yielded from TRS were characterized using scanning electron microscopy (SEM).

## Results and discussion

*Hardness measurements*

The measured Hv-values of Cu-Sn alloys were presented in **Table 1**. As shown in **Table 1**, Sn content has a strong

effect on Cu-Sn alloys hardness. The addition of 5% Sn resulted in increasing the Hv-values of the alloy by 8.6 %. Moreover, increasing the Sn percentage up to 15 % resulted in further increase of the alloy Hv-values by 26.2%. The Sn was an affecting agent in ameliorating the micro-hardness of the Cu alloys; which could be attributed to the massive precipitations of $Cu_3Sn$, which results in lattice distortions through acting as a barrier for dislocation motion; therefore, an effective delay in grain-boundary sliding could take place. In addition, increasing the Sn percentage resulted in increasing the volume fraction of the $Cu_3Sn$, which leads to increase the hardness of alloys. The strengthening mechanisms associated with Sn addition are various and may include solid solution strengthening, secondary phase strengthening, grain refinement strengthening, and grain boundary strengthening.

**Table 1.** Mechanical properties of the hot-pressed Cu–Sn alloys.

| Cu-Sn Alloy | Hv | Yield Strength ($\sigma_y$) | Ultimate Strength (UCS) | Fracture Strain % ($\varepsilon_f$) | Impact Energy Joule |
|---|---|---|---|---|---|
| Cu-0%Sn | 95 | 221 | 243.3 | 18 | 40.1 |
| Cu-5%Sn | 103 | 169.8 | 230.19 | 16 | 43 |
| Cu-10%Sn | 109 | 123.4 | 216.5 | 12.5 | 46.3 |
| Cu-15%Sn | 117 | 96.71 | 191.29 | 10 | 47.6 |

*Compression test measurements*

Strength and ductility were substantially affected by the addition of Sn particles. In addition, brittle fracture was observed. Comparison of the yield strength, ultimate strength, and the elongation percentages at the fracture for the tested materials, produced by hot pressing PM technique, were presented in **Table 1**.

It is clear that the tensile properties of Sn-containing alloys decrease with an increase in Sn content and that they are lower as compared to Sn-free alloys. As listed in **Table 1**, increasing the Sn percentage resulted in a dramatic reduction in the yield strength. Addition of 5 % Sn revealed a reduction of the Cu-Sn alloy by 23%. Increasing the Sn percentage up to 15 % resulted in a severe reduction in the yield strength (56 % compared to 100%Cu–0%Sn alloy). The ultimate compressive strength and the ductility exhibit a similar behavior. This decrease of the compression test data is related to the extreme addition of Sn, which is correlated to a higher coarsening rate of $Cu_3Sn$ and $Cu_6Sn_5$ precipitations [**33**]. The aggregation of coarse $Cu_3Sn$ and $Cu_6Sn_5$ precipitations at grain boundaries would take the role of the origin of cracks; therefore, it would have a damaging effect on the ultimate strength and the ductility. In addition, the poorer strength alloys may be attributed to the development of a soft phase, developed; mainly, on the grain boundaries by heat treatment. On the other hand, adding Sn extremely lead to the increase in percentage of the void, this was expected to happen along the development of $Cu_3Sn$ and shaped around the coarse precipitates near the surface,

resulting in crack initiation. The possible reason for reduced strength and ductility of alloys with Sn was the increase of area percentage porosity compared to Sn-free alloy. The reduction in strength and ductility of alloys with Sn could be attributed to the increase of area percentage porosity compared to Sn-free alloy. It may be concluded that the reduction trend in compression test data for Cu-Sn alloys is related to the negative effects of porosity that overcome the positive effects of $Cu_3Sn$ and $Cu_6Sn_5$ precipitates.

*Transverse rupture strength*

The TRS measurements for Cu-Sn alloys are presented in **Table 1**. As the total absorbed energy is normally taken to represent the impact energy, this parameter will be mainly used to discuss the impact properties in relation to the addition of Sn. The impact total energy is composed of two energy values, where impact energies are absorbed by the test specimens during damage initiation ($E_i$) and damage propagation ($E_p$) stages ($E_T = E_i + E_p$); therefore, these two values may also be defined as toughness parameters. The impact energy of the Sn-free alloy was improved from 40.1 to 43 J corresponding to an addition of Sn with 5%, where this improvement represents an increase of about 7.2%. Further improvement by 18.7% had been revealed compared with the Sn-free alloys by increasing the Sn percentage up to 15%. It is clear that the improvement in the toughness is a consequence of the gradual improvement in $E_i$ and $E_p$ with the increase of Sn.

The addition of Sn would lead to an enhancement in toughness, which reveals the sensitivity of alloy behavior to microstructural variations and it also highlights the significance of the fineness and softness of Sn in the toughness values [**33**]. On the other hand, excessive use of Sn in Cu-Sn alloys, obtained in brittle mechanism as expected under dynamic loading, is a result of the predominant effect of the Sn phases on the rupture of the alloy; moreover, the voids formation is a result of $Cu_3Sn$ and $Cu_6Sn_5$ precipitates, which are caused from brittle fracture due to its root brittle nature and propensity to produce structural defects.

*Fracture surface*

Cu particles coated with thin Sn had a relative small size, irregular shape, and tendency to agglomerate. The Cu phase was spread in many pools or lakes present in the compression fractured samples. The high hardness may be attributed to the process of continuous crystallization during the plastic deformation. Cu–Sn alloys have been observed to undergo mechanically induced fine crystallization; whereas, fine crystal precipitation in Cu–Sn alloys was also observed within vein protrusions on the compression fracture surface and along crack propagation paths; as well as, within shear bands resulting from bending. The weight percentages of alloys with compositions of 100%Cu–0%Sn, 95%Cu–5%Sn, 90%Cu–10%Sn, and 85%Cu–15% Sn; respectively, disclosed a seemingly classical inclined multi-shear fracture surface along the applied stress axis, which was alike to what was met for a diversity of hard metals, as presented in **Fig. 3 [34-35]**.
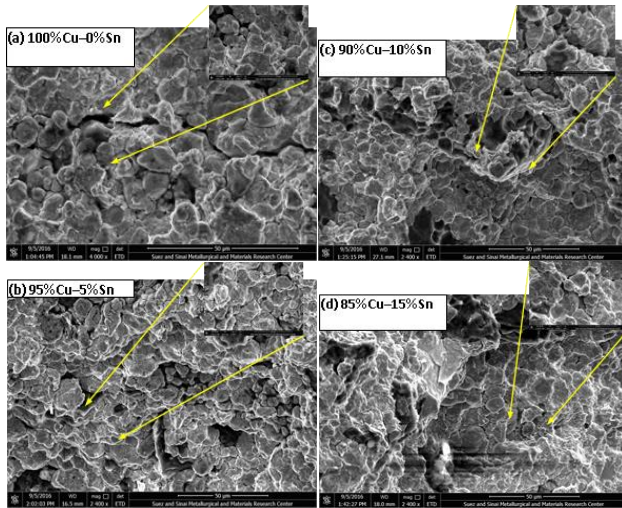
**Fig. 3.** SEM image of irregularities and rough morphologies of the fracture surface for compression fractured of (a) 100%Cu–0%Sn alloy, (b) 95%Cu–5%Sn alloy, (c) 900%Cu–10%Sn alloy, and (d) 85%Cu–15%Sn alloy, with higher magnifications.

Evidence of severe surface roughness was spotted, as shown in the higher magnifications of the fracture surface of 90% Cu–10% Sn and 85% Cu–15% Sn alloys, as presented in **Fig. 3c, d**, where the surface roughness denoted less intensity in the case of 100% Cu–0% Sn and 95% Cu–5% Sn alloys, as presented in **Fig. 3a, b**. This could be related to the release of the load at the final event of fracture in this limited area. The fracture surface was linked to the formation of the very fine particles in the alloys, which enhances the homogeneity of the deformation leading to the formation of multiple shear planes; instead of a single shear plane, normally encountered in 90% Cu–10% Sn and 85% Cu–15% Sn alloys, as presented in **Fig. 3c, d**. Increasing tin in the copper based alloy resulted in a rougher fracture surface, which could be related to the different viscosity of the Cu, and Sn elements in the region. This leads to a less critical shear stress and a more readily plastic deformation.

Rougher stress components parallel to the surface are obtained from the difference in multi-shear planes with deviation in fracture angles, which successively has a significant importance in the fracture process. The obtained fracture mechanism of the under-study materials involved plastic deformation of binder phase and brittle cracking of tin grains and copper network **[34]**. As a result, increasing the content of binder (Sn) increased roughness as shown in **Fig. 3c, d** (higher Sn content) compared to **Fig. 3a, b** (low Sn content); whereas, materials with higher amount of Sn in the microstructure exhibit higher fracture resistance **(see Table 1.)**, due to the higher bulk hardness; on the other hand, lower binder content leads to lower fracture resistance, where brittle cracking of Sn grains occurs.

## Conclusion

The Cu–Sn powder alloys were successfully fabricated using hot pressing technique followed by liquid-phase sintering process. It was found that, the hot-pressed specimens of Cu–Sn alloys included intermetallic phases,

which were homogeneously distributed. In addition, increasing the Sn weight percentage up to 15% resulted in increasing hardness values, reducing the yield strength, and increasing the impact energy by 26.2, 23, and 18.7%, respectively, in comparison with the Sn-free alloy. The Cu-Sn alloys showed an apparent classical inclined fracture surface, about 45°, with the applied stress axis, which was similar to that encountered for a variety of hard metals. Accordingly, increasing the Sn percentage resulted in the increase of the surface roughness at the fracture surface of the Cu-Sn alloys samples.
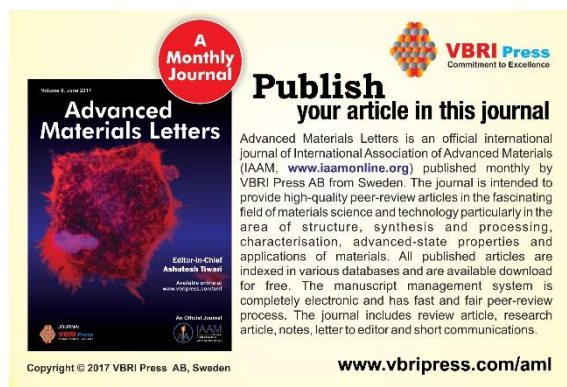
## Author's contributions

All authors have equal contributions. Authors have no competing financial interests.

**References**

1. Lee, J.J; Kim, B.J.; Min, W.S.; *Journal of Alloys and Compounds*, **1993**, 202, 237-242.
   **DOI:** 092583889390545X
2. Lu, K; *Science*, **2010**, *328*, 319-320.
   **DOI:** 10.1126/science.1185866
3. Shin, J.H; Park, J.S.; Bae, D.H.; *Met and Mater. Int.*, **2011**, 17(3), 441-444.
   **DOI:** s12540-011-0622-1
4. Jun, L.; Ying, L.; Lixian, L. Xuejuan, Y.; *Composites Part B: Engineering*, **2012**, 43(4), 1681-1686.
   **DOI:** S1359836812000418
5. Juskenas, R.; Mockus, Z.; Kanapeckaite, S.; Stalnionis, G.; Survila, A.; *Electrochimica Acta*, **2006**, 52, 928–935.
   **DOI:** S0013468606006980
6. Kang, Y.; Park, J. Kim, D.W.; Kim, H.; Kang, Y. C.; *Applied Surface Science,* **2016**, 389,1012-1016.
   **DOI:** 10.1016/j.apsusc.2016.08.041
7. Lei, C.; Huang, H.; Huang, Y.; Cheng, Z.; Tang, S.; Du, Y.; *Powder Technology*, **2016**, 301, 356-359.
   **DOI:** S0032591016303618
8. Jordan, M.; Modern Electroplating; John Wiley & Sons: USA, **2010**.
   **DOI:** productCd-0470167785
9. Ceylan, M.; Zengin, R.; *Journal Materials Processing Technology,* **2000**, 97 (1-3), 148-152.
   **DOI:** S0924013699003817
10. F.S. Ke, F.S.; Huang, L.; Cai, J.S.; Sun, S.G.; *Electrochim. Acta,* **2007**, 52 (24), 6741-6747.
    **DOI:** S0013468607006123
11. Dogan, M.; Olgar, M.A.; Cengiz, E.; Tıraşoglu, E.; *Radiation PhysicsandChemistry*, **2016**, 126, 111-115.
    **DOI:** 10.1016/j.radphyschem.2016.05.019
12. Finazzi, G.A.; de-Oliveira, E.M.; Carlos, I.A.; *Surface & Coatings Technology*, **2004**, 187, 377- 387.
    **DOI:** S0257897204000532
13. Tan, M.; Xiufang, B.; Xianying, X.; Yanning, Z.; Jing, G.; Baoan, B.; *Physica B*, **2007**, 387, 1-5.
    **DOI:** S0921452605013086
14. Liu, J.H.; Zhao, H.Y.; Li, Z.L.; Song, X.G.;  Dong, H.J.; Zhao, Y.X.; Feng, J.C.; *Journal of Alloys and Compounds*, **2017**, 692(25), 552-557.
    **DOI:** S0925838816326639
15. Liu, B.; Tian, Y.; Wang, C.; An, R.; Liu, Y.; *Journal of Alloys and Compounds*, **2016**, 687, 667-673.
    **DOI:** S0925838816319120
16. Ji, H.; Qiao, Y.; Li, M.; *Scr. Mater.*, **2016**, 110, 19-23.
    **DOI:** S1359646215003279
17. Qiao, X.; Corbin, S.F.; *Materials Science and Engineering A*, **2000**, 283, 38-45.

**DOI:** S0921509300006213

18. Shen, J.; Campbell, L.; Suri, P.; German, R.M.; *International Journal of Refractory Metals & Hard Materials*, **2005**, 23, 99-108.
    **DOI:** S026343680400071X

19. Nikolic, Z. S.; Yoshimura, M.; *Mathematical and Computer Modelling*, **2010**, 51, 1140-1145.
    **DOI:** S0895717709004579

20. Corbin, S.F.; Mc-Isaac, D.J.; *Materials Science and Engineering A*, **2003**, 346, 132-140.
    **DOI:** S0921509302005300

21. Lu, P.; Xu, X.; Yi, W.; R.M. German, R.M.; *Materials Science and Engineering A*, **2001**, 318, 111-121.
    **DOI:** S0921509301013302

22. Klar, E.; Samal, P.K.; *ASM International*, **2007**, 59-100.
    **DOI:** 56/10192/05200G/PUBLICATION

23. Córdoba, J. M.; Chicardi, E.; Gotor, F.J.; *Journal of Alloys and Compounds*, **2013**, 559, 34-38.
    **DOI:** S0925838813000728

24. Yunzhu, M.; Jiajia, Z.; Wensheng, L.; Yaxu, Z.; *Rare Metal Materials and Engineering*, **2014**, 43(9), 2108-2111.
    **DOI:** S1875537214601582

25. German, R.M.; Suri, P.; Park, S.J.; *J. Mater. Sci.*, **2009**, 44, 1-39.
    **DOI:** s10853-008-3008-0

26. Olevsky, E.A.; German, R.M.; *Acta Mater.*, **2000**, 48, 1153- 1166.
    **DOI:** S1359645499003687

27. Upadhyaya, A.; German, R.M.; *Materials Chemistry and Physics*, **2001**, 67, 25-31.
    **DOI:** S0254058400004156

28. Namini, A.S.; Azadbeh, M.; Mohammadzadeh, A; *Science of Sintering*, **2013**, 45, 351-362.
    **DOI:** 10.2298/SOS1303351S

29. German, R.M.; *Metallurgical and Materials Transactions A*, **1997**, 28(7), 1553-1567.
    **DOI:** s11661-997-0217-0

30. Tongsri, R.; Tosangthum, N.; Yotkaew, T.; Muthitamongkol, P.; Sri-on, A.; Patakham,U.; *Materials Characterization,* **2016**, 113, 52-59.
    **DOI:** S1044580316300018

31. El-Katatny, S.M.; Nassef, A.E.; El-DomiatyA.; El-Garaihy, W.H.; *International Journal of Engineering and Technical Research*, **2015**, 3(3), 180-184.
    **DOI:** IJETR031605

32. Koval'chenko, M.S.; *Powder Metallurgy and Metal Ceramics,* **2009**,48(3), 133-144.
    **DOI:** s11106-009-9118-7

33. Mohamed, A.M.A.; Samuel, F.H.; Samuel, A.M.; Doty, H.W.; Valtierra, S; *Metallurgical and Materials Transactions A*, **2008**, 39A, 490-501.
    **DOI:** s11661-007-9454-5

34. Nassef, A.; El-Hadek, M.; *Advances in Materials Science and Engineering*, **2016**, 1-10.
    **DOI:** org/10.1155/2016/9796169

35. El-Hadek, M. Kaytbay, S.; *Metallurgical and Materials Transactions A*, **2013**, 44(1), 544-551.
    **DOI:** s11661-012-1396-x